Chinese Journal of Oceanology and Limnology
Vol.21, No.3, P.193 - 213, 2003

Determination of the Current System on Isopycnal Surface Between Mindanao and New Guinea from GDEM *

Peter C Chu, LI Rongfeng†, FAN Chenwu
(*Naval Ocean Analysis and Prediction Laboratory Department of Oceanography, Naval Postgraduate School-Monterey, CA 93943, USA*)
(*†LASG, Institute of Atmospheric Physics, Chinese Academy of Sciences, Beijing 100080, China*)

Received May 30, 2002; revision accepted Nov. 21, 2002

Abstract In this study, we used the Navy's Generalized Digital Environmental Model (GDEM) climatological temperature and salinity data on a $0.5° \times 0.5°$ grid to investigate the seasonal variabilities of the southwest Philippines Sea ($0.5° - 9°N$, $123.5° - 136.5°$) thermohaline structure and circulation. The GDEM for the area was built up on historical (1930 - 1997) temperature and salinity profiles. A three-dimensional estimate of the absolute geostrophic velocity field on isopycnal surface was obtained from the GDEM temperature and salinity fields using the P-vector method. The seasonal variabilities of the thermohaline structure and currents (obtained from the inverse method) such as the Mindanao Current, Mindanao Undercurrent, North Equatorial Counter Current, New Guinea Coastal Undercurrent, and dual-eddies (cyclonic Mindanao Eddy and anticyclonic Halmahera Eddy) are identified.

Key words: current system, isopycnal surface, GDEM

1. INTRODUCTION

The western equatorial Pacific, particularly the southernmost Philippine Sea, was called "water mass crossroads" by Fine et al. (1994) due to the confluence there of several water masses from higher latitudes of both hemispheres (Wyrtki, 1961; Fine et al., 1994). Fine et al. (1994) depicted (Fig.1) major currents in the Indonesian region.

After encountering the western boundary along the Philippine coast, the North Equatorial Current (NEC) bifurcates into the northward flowing Kuroshio and the southward flowing Mindanao Current (MC) (Nitani, 1972). The MC and the New Guinea Coastal Undercurrent (NGCUC) flow equatorward, feeding the North Equatorial Counter Current (NECC), the New Guinea Coastal Current (NGCC), and the flow from the Pacific to the Indian Ocean, that is, the Indonesian Throughflow (IT). The MC is unique because it is the only northern hemisphere low-latitude western boundary current that has a mean flow toward the equator (Lukas et al., 1996), and is important because it feeds to IT (Ffield and Gordon, 1992), and impacts on the stratification of the Indian Ocean (Lukas et al., 1996; Godfrey, 1996).

* Peter Chu and Fan Chenwu were supported by the Office of Naval Research and the Naval Oceanographic Office. Li Rongfeng was supported by NSFC (40076009), and Chinese Academy of Sciences (KZCX2-204, KZCX1-SW-01-16).

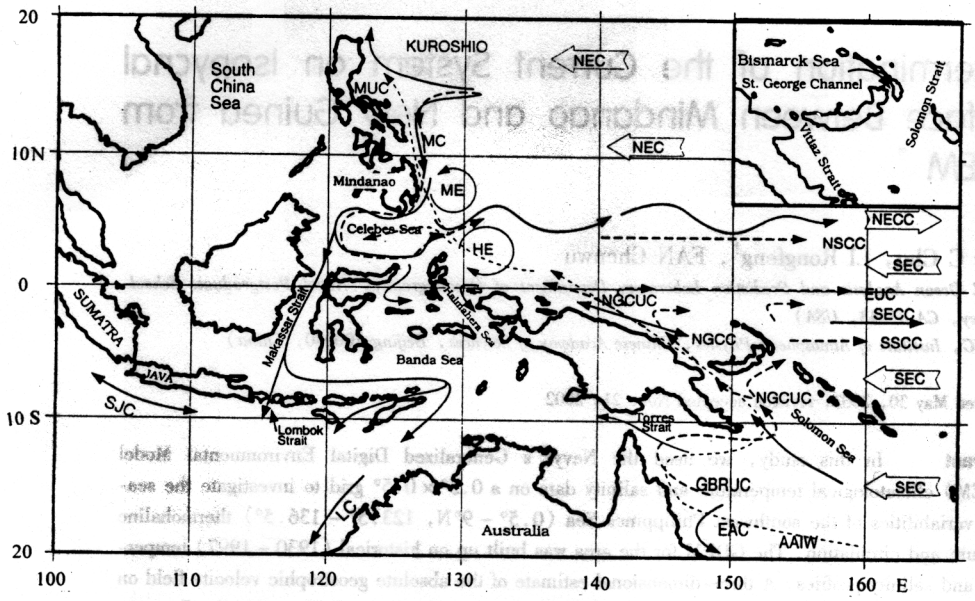

Fig.1 Map of the western tropical Pacific Ocean and Indonesian Seas showing the major geographic names and surface to intermediate depth currents. Here ME and HE represent Mindanao and Halmahera eddies (after Fine et al., 1994)

The NECC divides into three branches near 130°E. The central branch continues to flow eastward as the NECC. The northern branch moves northwestward and forms a cyclonic eddy near Mindanao Island, and is called the Mindanao Eddy (ME). The southern branch moves southwestward, joins the northwest moving currents from NGCC and NGCUC, which are parts of the South Equatorial Current (SEC), and forms an anticyclonic eddy called Halmahera Eddy (HE) near the Halmahera Sea.

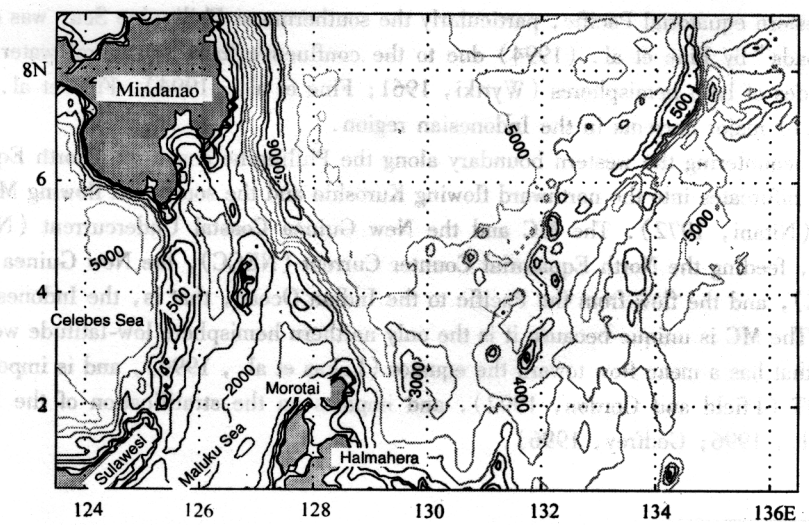

Fig.2 Geography and isobaths showing the bottom topography of the southwestern Pacific near Mindanao Island

Metzger and Hurlburt (1996) adopted a high horizontal resolution six-layer model driven by monthly climatological winds to analyze the coupled dynamics among the Sulu Sea, the South China Sea, and the Pacific Ocean. Their model simulates the existence of the dual eddy (ME and HE) structure in the middle of the "water mass crossroads" surrounded by complicated topography (Fig. 2), and connected to major equatorial currents. Seasonal variabilities (thermohaline structure and circulation) of the two eddies represent the seasonal variability in the low latitude dynamics and interbasin water mass exchange.

Water mass characteristics had been used to infer flow along isopycnal surfaces. For example, between 300 and 1000 m the North Pacific Intermediate Water (NPIW) (around $\sigma_\theta = 26.8$) and Antarctic Intermediate Water (AAIW) (around $\sigma_\theta = 27.2$) reach this area (Reid, 1965; Tsuchiya, 1991; Tally, 1993; Bingham and Lukas, 1994, 1995; Fine et al., 1994). Kashino et al. (1996) confirmed the existence of NPIW and AAIW in the far western equatorial Pacific near the entrances to the Celebes and Halmahera Seas. They also provided further evidence for the flow of waters from the southern hemisphere across the equator, turning eastward into NECC.

To obtain current signal quantitatively from hydrographic data in this area is not easy. Godfrey (1996) pointed out that there are a number of special difficulties such as active internal tides and the fact that the geostrophy can only be used with caution to estimate the current distribution in the area. To overcome these difficulties, we used the P-vector method on the isopycnal surfaces (Chu, 1995, 2000; Chu and Li, 2000; Chu et al., 1998, 2001a,b) to invert the absolute velocity from the Navy's public domain Global Digital Environmental Model (GDEM) climatological monthly mean temperature and salinity data set with $1/2° \times 1/2°$ resolution (Teague et al., 1990). The P-vector method is a two-step inverse method for determining first the direction of the current (P-vector) and then the magnitude using the thermal wind relation. The two necessary conditions for validity of inversion are easily incorporated into the P-vector method (Chu et al., 1998).

We investigated the seasonal variabilities of the three-dimensional circulation and thermohaline structure of the dual eddies (ME and HE). The rest of the paper is outlined as follows: Section 2 describes the GDEM T, S data in the isopycnal coordinate system. Section 3 depicts the monthly mean velocity fields calculated using the P-vector method. Section 4 discusses the seasonal variability of the volume transport streamfunction. Section 5 presents the conclusion.

2. ISOPYCNAL COORDINATE SYSTEM

Vertical discretization

The GDEM T, S dataset showed that the potential density σ_θ varies from 22.2 to 27.725. We discretized σ_θ with the increment $\Delta\sigma = 0.025$ kg/m^3 to obtain 222 σ_θ-layers within which the density is vertically uniform. To resolve well the isopycnal surfaces, we used cubic spline to interpolate the T, S data into 246 z-levels with three different increments: 5 m from 0 to 100 m depth, 10 m from 100 to 1000 m depths, 20 m from 1000 to 2500 m depths, and 50 m below 2500 m depths. Thus, we built up a high resolution z-coordinate dataset $[T(z_j), S(z_j), \sigma_\theta(z_j)]$. Notice that the value of 27.725 is the maximum value for σ_θ, computed from the GDEM T, S dataset.

Transformation of T, S data from z-coordinates to σ_θ-coordinate system

The transformation was done by comparing the z-coordinate potential density data $\hat{\sigma}_\theta(z_j)$ with

the discrete σ-values, $\sigma(k)$. The two values refer to different dimensions. $\hat{\sigma}_\theta(z_j)$ for the depth-z_j, and $\sigma(k)$. Thus, we use the sigma value at the bottom of the kth isopycnal layer, $\sigma^b(k)$ for the comparison,

$$\sigma^b(k) = \frac{1}{2}[\sigma(k) + \sigma(k+1)] \tag{1}$$

The depth of the bottom of the $\sigma(k)$-layer is obtained by

$$\hat{z}_k^{(\sigma)} = z_j, \quad \text{if} \quad \hat{\sigma}(z_j) = \sigma^b(k) \tag{2}$$

and

$$\hat{z}_k^{(\sigma)} = z_j + \frac{\sigma(k) - \hat{\sigma}(z_j)}{\hat{\sigma}(z_{j+1}) - \hat{\sigma}(z_j)}(z_{j+1} - z_j), \quad \text{if} \quad \hat{\sigma}(z_j) < \sigma^b(k) < \hat{\sigma}(z_{j+1}) \tag{3}$$

where the superscript b indicates the bottom of the kth isopycnal layer. The thickness of the kth isopycnal layer is obtained by

$$\hat{h}_k^{(\sigma)} = \hat{z}_{k-1}^b - \hat{z}_k^b \tag{4}$$

After $\hat{h}_k^{(\sigma)}$ is obtained, we may compute the potential vorticity on the isopycnal surface, and then use the P-vector method to compute the absolute velocity (Chu and Li, 2000; Chu et al., 2001c).

Bi-monthly mean thermohaline fields on $\sigma_\theta = 25.0$ kg/m^3

In the pycnocline layer (100 to 300 m) are salinity maximum layers from the North and South Pacific. These water masses were called North Pacific Tropical Water (NPTW) and South Pacific Tropical Water (SPTW) by Kashino et al. (1996). It is not our intention to present a detailed climatological thermohaline structure in this paper. We only show some representative features on σ_θ = 25.0 kg/m^3 (pycnocline) as illustration. This level is generally considered to be where the salinity maximum occurs (Kashino et al., 1996).

Temperature The bi-monthly mean temperature on $\sigma_\theta = 25.0$ (Fig.3) shows a cool (northern)-warm (southern) eddy-like structure with strong seasonal variability. The cool (warm) eddy is enclosed by the 18.25 (20℃) isoline. The cool eddy shows up almost all year round and is located at 128° – 133°E and 6° – 9°N, and the warm eddy is evident only in winter (February) and spring (April). A weak thermal front exists between the cool and warm eddies with horizontal temperature gradient of less than 1℃/100 km. This front strengthens from December to April, and weakens from April to December.

Salinity Salinity is generally used for identifying the water masses in the area. For example, Kashino et al. (1996) used the 35.0 psu contour as the boundary of high salinity SPTW in analyzing data collected by the *R/V Kaiyo* during the World Ocean Circulation Experiment (WOCE) expedition I in October 1992 and II in February 1994. Both expeditions covered the same area as ours (Fig.4). Horizontal distribution on $\sigma_\theta = 25.0$, observed during *Kaiyo* WOCE I and II, showed the high-salinity SPTW in the southern area. In October 1992, SPTW reached 2°N near Morotai Island and 3°N along 134°E (Fig.4a). In February 1994, SPTW reached farther north than in October 1992 (Fig.4b), i.e., north of Morotai Island and 5°N along 130°E (Kashino et al., 1996).

The monthly mean salinity on $\sigma_\theta = 25.0$ (Fig.5) shows feature similar to that depicted by Kashino (1996). The high-salinity SPTW (35.0 psu) is located in the southern part of the area, and expands toward the northwest in Feb.-Jun., and retreats toward the southeast in August-December. SPTW has the largest penetration in February – April. The boundary of SPTW is at 2° – 3° N near Morotai Island (128°E), reaches northernmost (5°N) at 131°E, and southward turns to 3°N at 136°E. In February and April, a high salinity center enclosed by 35.3 psu occurs at 131° – 133°

E, 1° – 3°N, which coincides with the warm center (Fig.3).

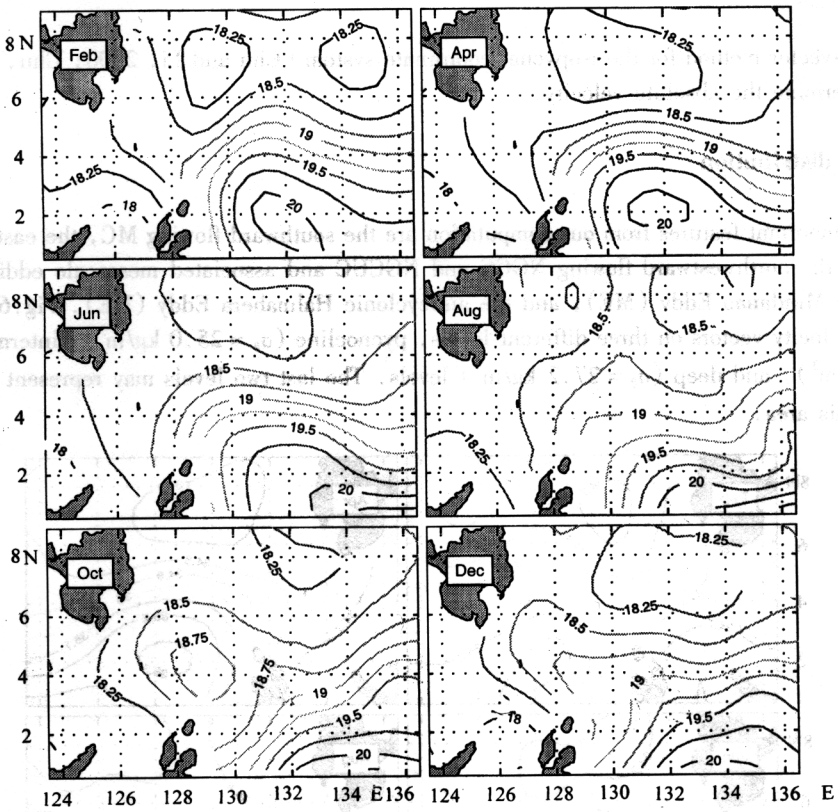

Fig.3 Bi-monthly mean temperature (℃) fields on $\sigma_\theta = 25.0$ kg/m^3 from GDEM

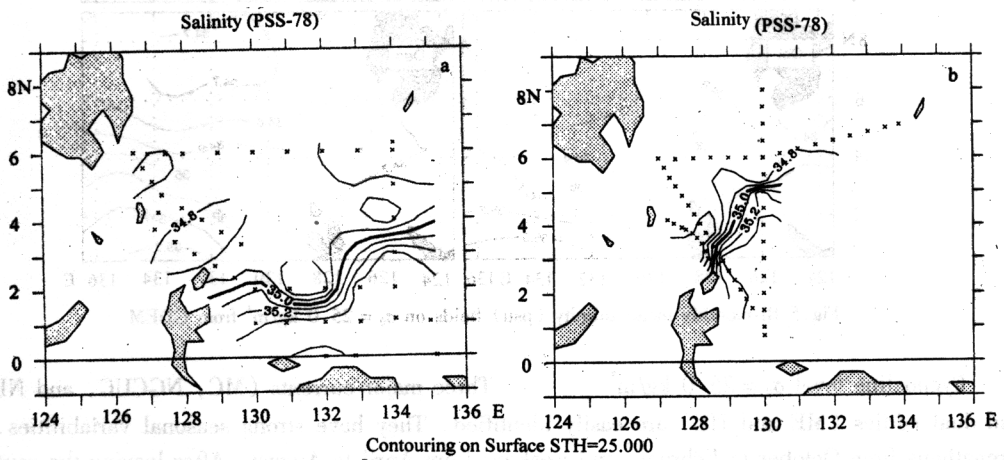

Fig.4 Salinity distributions on the surface $\sigma_\theta = 25.0$ kg/m^3 during (a) *Kaiyo* WOCE I and (b) *Kaiyo* WOCE II (from Kashino et al., 1996). The observation stations are marked by "×"

3. VELOCITY FIELD

The P-vector method for the isopycnal coordinate system (Chu and Li, 2000; Chu, 2001) was used to determine the absolute velocity.

Horizontal distribution

Most important features from our computation are the southward flowing MC, the eastward flowing NECC, the northwestward flowing NGCC and NGCUC and associated mesoscale eddies such as the cyclonic Mindanao Eddy (ME), and the anticyclonic Halmahera Eddy (HE). Fig.6 shows the horizontal velocity vectors on three different-levels. pycnocline ($\sigma_\theta = 25.0$ kg/m^3), intermediate ($\sigma_\theta = 26.5$ kg/m^3), and deep ($\sigma_\theta = 27.2$ kg/m^3) levels. The last two levels may represent NPIW and AAIW in this area.

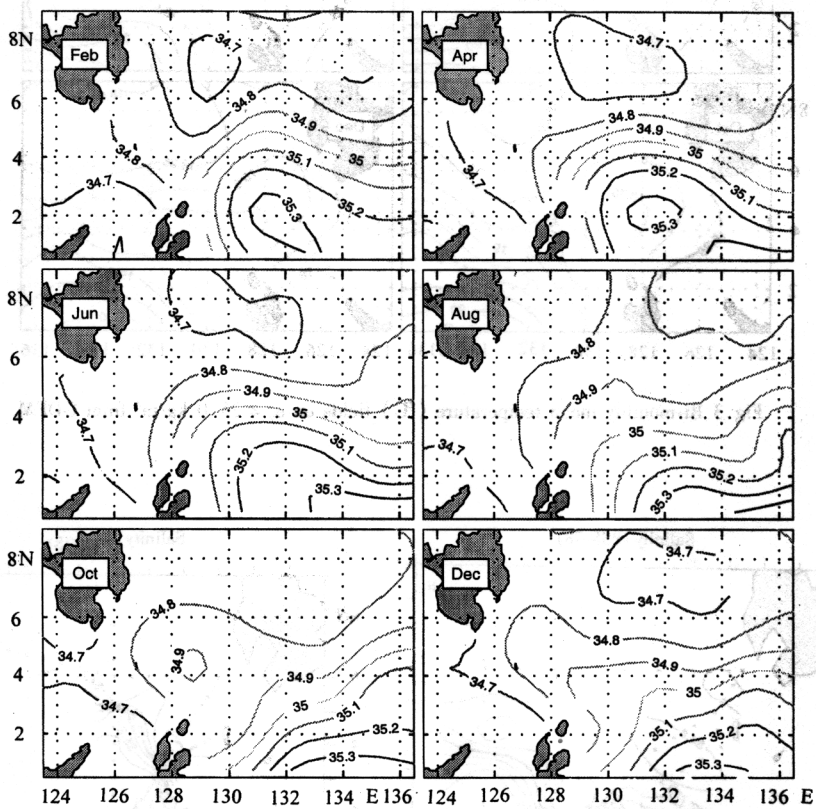

Fig.5 Bi-monthly mean salinity (psu) fields on $\sigma_\theta = 25.0$ kg/m^3 from GDEM

Pycnocline level $\sigma_\theta = 25.0$ kg/m^3 Three major currents (MC, NGCUC, and NECC) and dual eddies (ME and HE) are easily identified. They have strong seasonal variabilities. MC strengthens from October to February and weakens from April to August. After leaving the south tip of Mindanao Island, MC flows southeastward following the continental slope (Figs 12 and 2) and recirculates northeastward near Morotai Island. Such a recirculation leads to the formation of a cyclonic eddy, ME. The MC is very weak from April to August, strengthens in October, and becomes strong

in the winter with a maximum speed of around 0.25 m/s in February. NGCUC flows northwestward along northern New Guinea Island (Fig.1). After leaving the north tip of New Guinea Island, it continues to move northward and feeds an anticyclonic eddy, HE. This eddy strengthens in summer

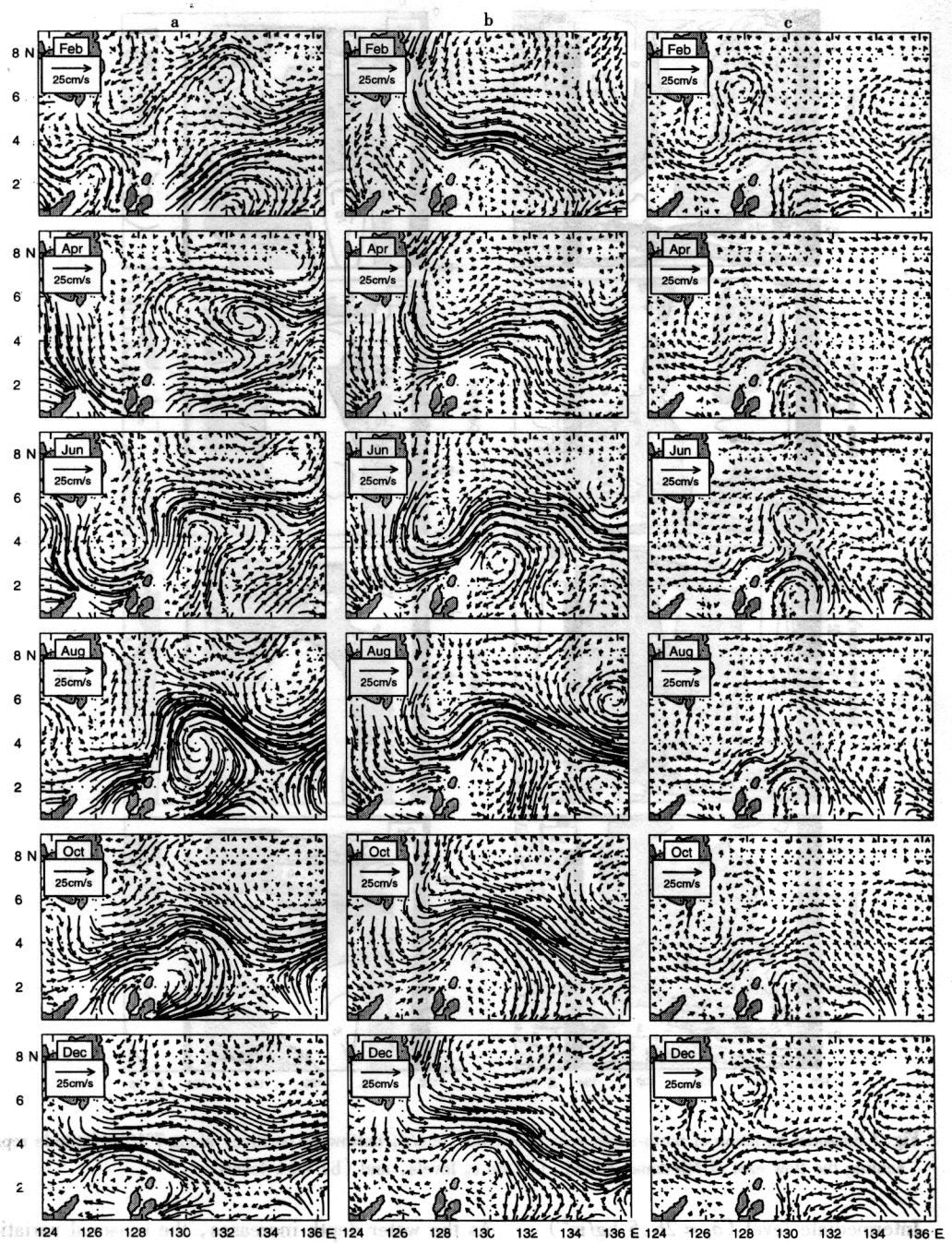

Fig.6 Bi-monthly mean velocity vector field east of Mindanao Island on the surface of (a) $\sigma_\theta = 25.0$ kg/m^3, (b) $\sigma_\theta = 26.5$ kg/m^3, and (c) $\sigma_\theta = 27.2$ kg/m^3

(June – August) and weakens in winter (December). In August, the HE is located at 128° – 133° E, 2° – 6°N with a maximum tangential velocity of around 30 cm/s.

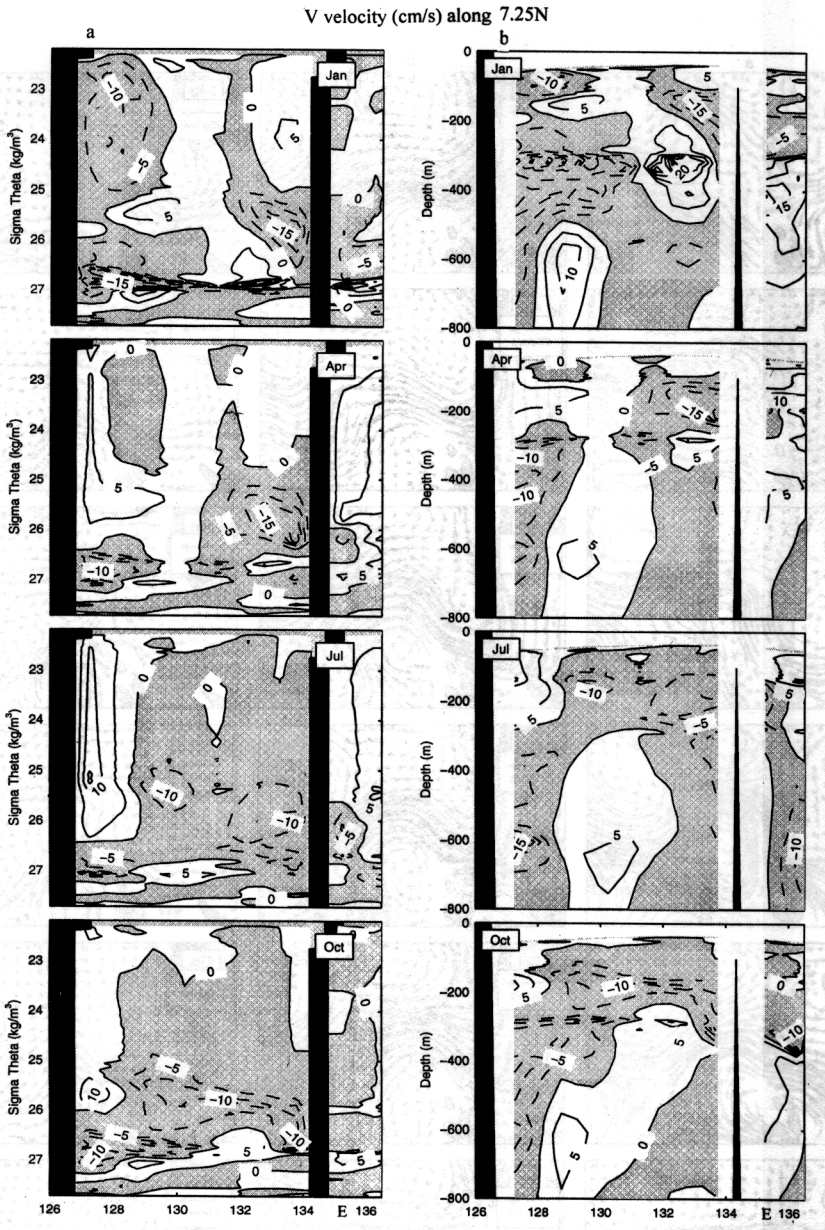

Fig.7 Seasonal variation of north-south velocities (unit. cm/s; northward positive) along 7°15′N latitude representing the flow east of Mindanao Island. (a) on σ_θ levels, and (b) on z levels

Intermediate level ($\sigma_\theta = 26.5$ kg/m^3) As the water depth increases, the seasonal variation of the velocity reduces. The intermediate level ($\sigma_\theta = 26.5$) is close to the level ($\sigma_\theta = 26.8$ kg/m^3) where NPIW located. The MC is an energetic, nearly 150 km wide, southward, coastal trapped jet. It turns east after leaving Mindanao Island and feeds into the NECC, which separates into three

branches near 130°E. The north and south branches feed into two eddies. cyclonic eddy (ME) and anticyclonic eddy (HE). The central branch continues as the NECC. In the winter (December-February), the dual eddies are north-south oriented with ME (maximum tangential velocity around 15 cm/s located at 128° – 133°E, 6° – 9°N and HE (maximum tangential velocity around 25 cm/s located at 128° – 133°E, 0.5° – 4°N. In April, ME (HE) expands toward the southwest (northeast). In June, the dual eddies are east-west oriented with ME in the west and HE in the east. The size of both eddies are smaller in the summer than in the winter.

Deep level ($\sigma_\theta = 27.2$ kg/m^3) At the deep level ($\sigma_\theta = 27.2$ kg/m^3) where AAIW located, the flow pattern is quite different from that on the pycnocline and intermediate levels. An evidently westward flowing current is identified between 2° – 6°N which is in opposite direction to that of NECC on the pycnocline and intermediate level. The flow pattern clearly shows NGCUC entering the eastern part of the southern boundary (134° – 136°E) and flowing northwestward with a maximum velocity larger than 20 cm/s in the winter (December-February).

In the winter (December – February), NGCUC bifurcates at 133°E, 4°N into two branches (northward and westward). The northward branch recirculates at 6°N and forms an anticyclonic mesoscale eddy (around 200 km in diameter). The westward branch flows zonally (under NECC) to a longitude near 129°E, and splits into three branches moving southward, westward, and northward. The westward branch transports AAIW into the Celebes Sea. The northward branch turns to west at 8°N, recirculates along the west coast of Mindanao Island, and forms a cyclonic eddy (i.e., ME). In the summer (June – August), a 200 km diameter cyclonic eddy with maximum swirl velocity of 15 cm/s is identified southeast of the southern tip of Mindanao Island.

Major currents

MC (along 7°15'N) As we mentioned, the MC is a major current at the water mass crossroads and feeds to NECC and IT. The seasonal variability of MC affects the seasonal variability of NECC and IT, which, in turn, impact on the seasonal variability of ME (due to the NECC variability) and the Indian Ocean stratification (due to the IT variability).

We use the north-south geostrophic velocities on isopycnal surfaces along 7°15'N to represent the seasonal variability of MC (Fig.7a). Positive (negative) values show the poleward (equatorward) flow. The negative values (equatorward flow) are shaded by grey color. The top-to-bottom black vertical bars represent the islands. The small black bars at the top or the bottom represent that σ_θ does not reach the values there. The equatorward flowing MC has two jet-cores, located in the upper layer above the pycnocline (from the surface to $\sigma_\theta = 25.0$), and deep layer ($\sigma_\theta > 26.5$), respectively. The upper layer jet-core has strong seasonal variability. Evident equatorward MC occurs from December to March at a maximum speed of 10 cm/s in January and February and 5 cm/s in March near the east coast of Mindanao Island at $\sigma_\theta = 23.25$. MC disappears from April to November. The deep layer jet-core exists with weak seasonal variability all year round. Its strength reaches the maximum (> 25 cm/s) in the winter (February) and the minimum in the summer (June – August).

We convert the v-component on σ_θ to that on z levels (Fig.7b). The v-component on z-level also shows the upper layer (around 50 m) jet-core and the deep layer jet-core (300 – 600 m), respectively. A maximum speed of 100 cm/s in MC was measured along 7°N (Lukas et al., 1991) with the use of Acoustic Doppler Current Profilers (ADCP). The calculated absolute velocities from GDEM underestimate the actual velocities.

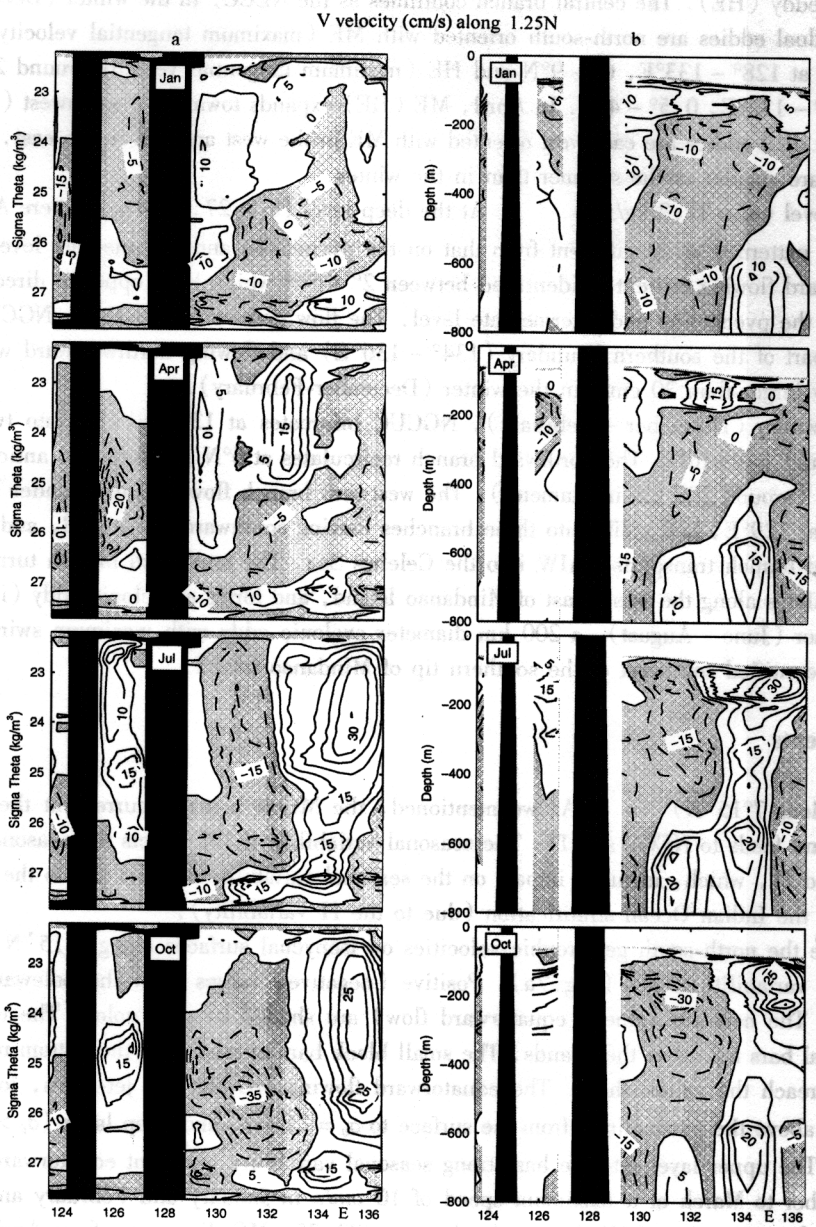

Fig.8 Seasonal variation of north-south velocities (unit: cm/s; northward positive) along 1°15′N latitude representing the flow east of Halmahera Island: (a) on σ_θ levels, and (b) on z levels

Fig.7b shows the existence of three northward velocity cores. Among them two cores are close to the coast (west of 130°E) and one core (centered at 300 m depth) is away from the coast (130° – 134°E). The two coastal cores represent the Mindanao Undercurrent (MUC) described by Hu and Cui (1989), and the third core represents the eastern part of the ME.

The MUC has evident seasonal variation. From April to September, the upper layer MUC, occurring from 50 to 300 m (centered at 200 m), is close to the coast and has a width of around 200 km and a maximum velocity of 10 cm/s. It retreats toward the coast from October to December with a width less than 100 km, and expands toward the east to a longitude near 132°E from January to March with a maximum velocity of 10 cm/s at around 150 m deep. The lower layer MUC, occurring below 400 m, is around 100 km away from the coast and has a weak seasonal variability in its location and a strong seasonal variability in its strength. It reaches a maximum strength (20 cm/s) in February and a minimum strength (5 cm/s) from March to October.

ME (Along 7°15'N) The ME is a sub-surface system, represented by the alternate southward flow west of and northward flow east of 130°E (Fig.7b). In November, the ME extends from 200 to 500 m with a jet core at 300 m depth. From November to March, its position keeps quite steady, but its strength varies drastically. The ME velocity enhances through February and weakens in March. The northward branch velocity increases to 20 cm/s in December and January, and the southward branch velocity increases to 25 cm/s in February. From April to October, the ME shifts southwestward to 128° – 133°E and south of 6°N (Fig.6).

NGCUC (Along 1°15'N) Similar to the MC, the NGCUC is a major current flowing from the Southern Hemisphere to the water mass crossroads and feeds NECC and IT. The seasonal variability of NGCUC affects the seasonal variability of NECC and IT, and, in turn, impacts on the seasonal variability of ME (due to NECC variability) and the Indian Ocean stratification (due to IT variability).

Since the geostrophic balance is not generally good, we use the computed v velocities on isopycnal surfaces along 1°15'N to calculate the seasonal variability of NGCUC approximately (Fig.8a). Positive (negative) values show the poleward (equatorward) flow. The negative values (equatorward flow) are shaded by grey color. Same as in Fig.7a, the top-to-bottom black vertical bars represent the islands. The vertical bars between 127°15′ and 128°45′E represent Halmahera Island (Fig.2). The small black bars at the top or the bottom represent that σ_θ does not reach the value there. The NGCUC has two branches; a 400 km wide coastal branch along the east coast of Halmahera Island and an around 300 km wide open water branch east of 133°E.

An interesting feature is the out-of-phase variation between the coastal and open water branches. For example, the coastal (open water) branch strengthens (weakens) from September to March, and the coastal (open water) branch weakens (strengthens) in spring from March to September. From January to April, the coastal branch is strong with two cores, one in the upper layer (above the pycnocline, i.e., $\sigma_\theta < 25.0$) and the other in the intermediate layer ($25.0 < \sigma_\theta < 26.5$). The maximum northward velocity is around 15 cm/s. The open water branch is located in the deep layer ($\sigma_\theta > 26.5$) and has maximum northward velocity of 15 cm/s. From April to October, the coastal (open water) branch weakens (strengthens) at a maximum northward velocity around 5 cm/s (40 cm/s in August). Besides, the open water branch extends from near surface to deep layer. Such an out-of-phase variation is also easily seen in the cross-section of the v-component on z level (Fig.8b).

NECC (Along 130°E) The NECC, originated from the confluence of southward flowing MC and northward flowing NGCUC, is an eastward equatorial flow centered at around 5°N (Lukas et al., 1991). We use the east-west geostrophic velocities on isopycnal surfaces along 130°E longitude to represent the seasonal variability of NECC (Fig.9a). Positive (negative) values show the eastward (westward) flow. The negative values (westward flow) are shaded in grey.

The NECC extends from the surface to the level of $\sigma_\theta = 27$ all year round. It occurs between 3° and 8°N from June to December and south of 8°N with two branches separated by an upper layer westward current from January to May, with two jet-cores, located in the pycnocline layer (centered

around $\sigma_\theta = 25.0$), and in the intermediate layer ($27.0 > \sigma_\theta > 26.0$), respectively. The pycnocline layer jet-core has strong seasonal variability and maximum speed of 40 cm/s (10 cm/s) in August (February). The intermediate layer jet-core is usually stronger than the pycnocline layer core with less seasonal variability. The maximum speed in the intermediate layer jet-core is 45 cm/s in February and 20 cm/s in May.

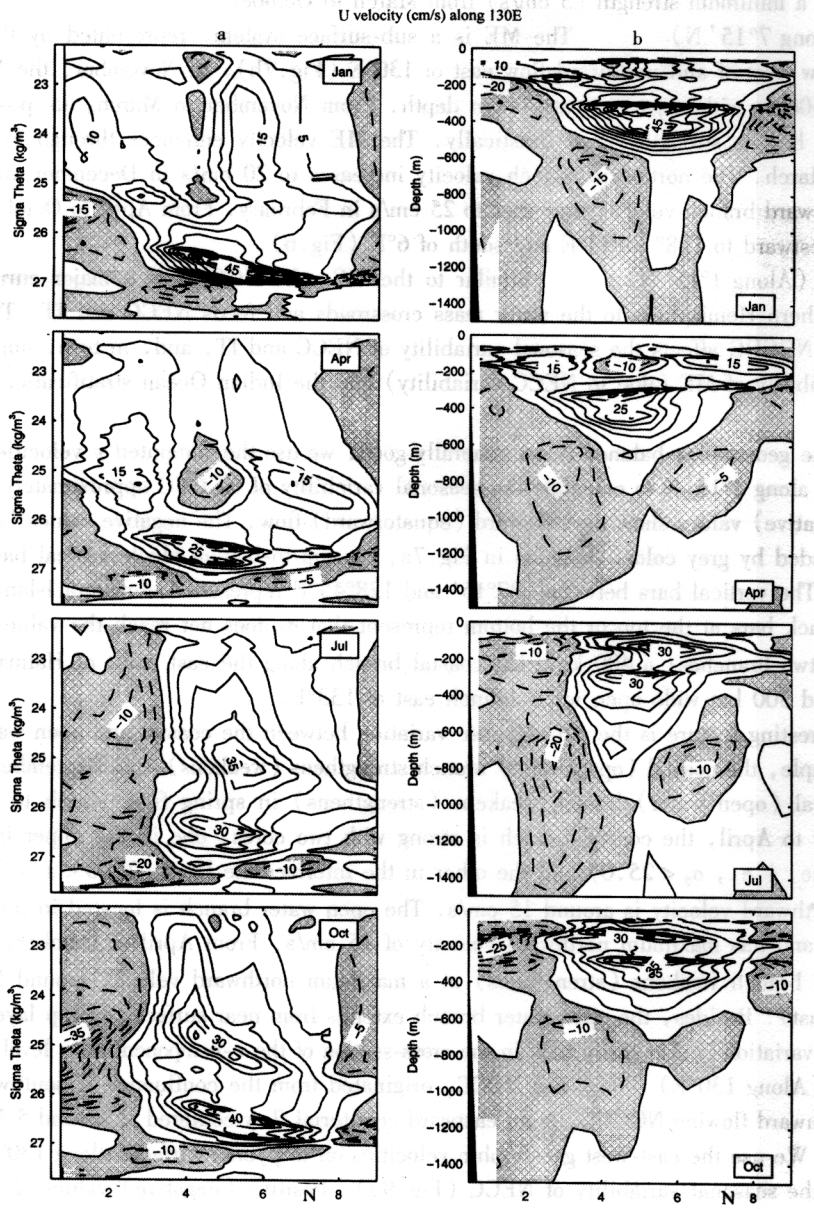

Fig.9 Seasonal variation of east-west velocities (unit. cm/s; eastward positive) along 130°E longitude representing NECC. (a) on σ_θ levels, and (b) on z levels

HE (Along 130°E) We convert the v-component on σ_θ to that on z levels (Fig.9b). The NECC separates near 130°E into three branches, central branch (continuation of NECC), north branch feeding to ME, and south branch feeding to HE. The HE is seen by the alternate eastward NECC and westward flow south of NECC. The strength of HE is represented by the velocity of the westward flow. The HE strengthens in summer (June – August) and weakens in winter (December). The maximum westward speed in the southern flank of the HE reaches 20 cm/s in June and July and 10 cm/s in February and March.

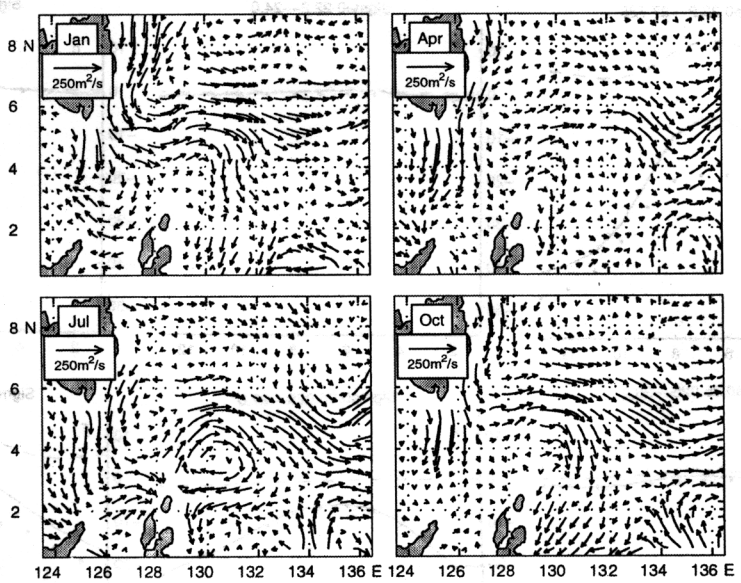

Fig.10 Vertically integrated velocity vectors

4. VOLUME TRANSPORT

Vertically integrated velocity

Monthly mean vertically integrated (for the whole water column) velocity is computed to represent the volume transport (Fig.10). Three major currents (MC, NGCUC, and NECC) and dual eddies (ME and HE) are also identified in the integrated flow field whose seasonal variation is evident. The integrated MC strengthens from October to February and weakens from April to August. After leaving the south tip of Mindanao Island, MC flows southeastward following the continental slope (Figs 16, 2) and recirculates northeastward near Morotai Island and then turns towards the east. The recirculation leads to the formation of ME (cyclonic eddy), and the eastward flow feeds into NECC. NGCUC flows northwestward into the area between 134° – 136°E at 0.5°N latitude and then joins the NECC at 133°E, 3°N. The ME-HE dipole pattern is evident from June to August.

MC volume transport

We computed monthly total and layered (between two σ_θ levels) volume transports across 7°15′ N (northward positive) between 126°45′ (Mindanao coast) to 130°45′E longitude (Fig. 11) to represent the seasonal variability of MC volume transport. The dashed, dotted, and solid curves indi-

cate northward, southward, and net transports. The northward flow is much weaker than the southward flow for the total transport and the most layered transports except the deep layer ($\sigma_\theta \geqslant 27.025$), where the northward flow is dominant. The total transport is negative (southward) all year round with a minimum value of -40.2 Sv in January and a maximum value of -5.3 Sv in June and July with annual mean of -23.4 Sv, which agrees with many existing estimates of -26, -20 Sv listed in Lukas et al. (1991, Table 1).

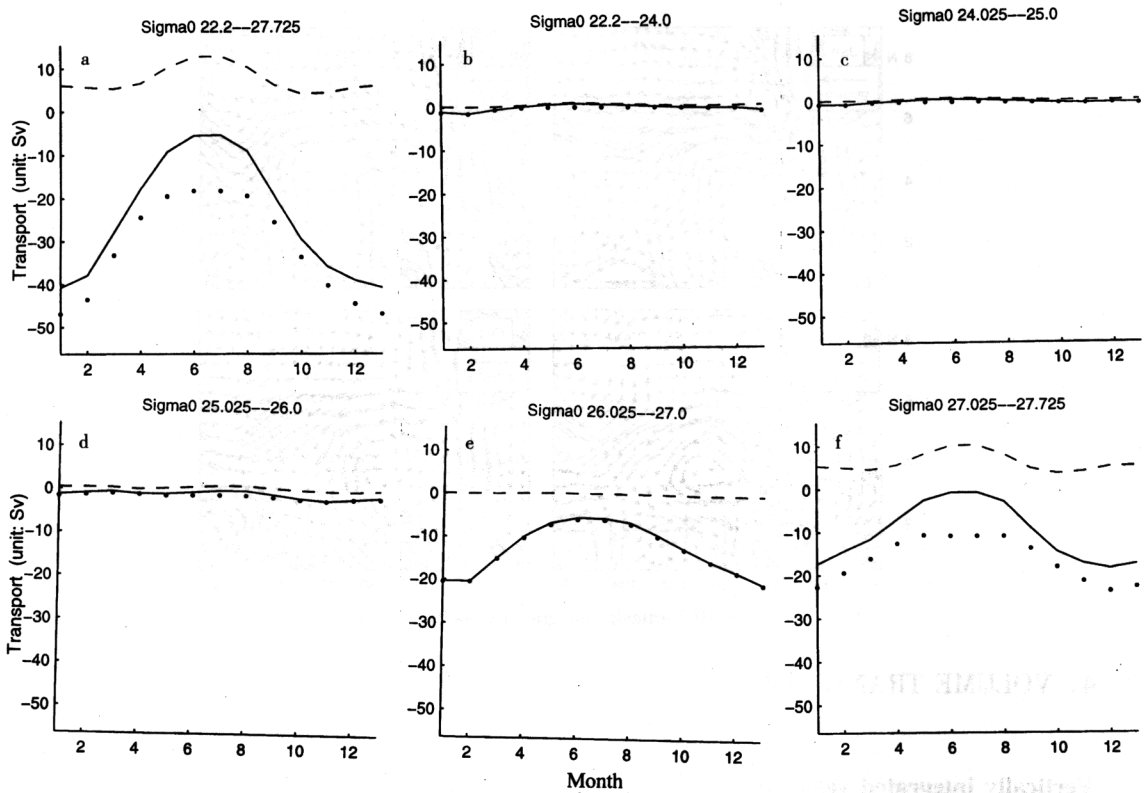

Fig.11 Monthly variation of total and layered (between two σ_θ levels) latitudinal volume transports (northward positive) across 7°15′N latitude between 126°45′ and 130°45′E, representing the MC transport (Sv). (a) total, (b) σ_θ less than 24.0, (c) σ_θ from 24.0 to 25.0, (d) σ_θ from 25.0 to 26.0, (e) σ_θ from 26.0 to 27.0, and (f) σ_θ more than 27.0. The dashed, dotted, and solid curves indicate the northward, southward, and net transports

NECC volume transport

We computed monthly total and layered (between two σ_θ levels) volume transports across 130° E (eastward positive) between 0°45′ and 6°15′N (Fig.12) to represent the seasonal variability of NECC volume transport. The dashed, dotted, and solid curves indicate eastward, westward, and net eastward transports. The westward flow is much weaker than the eastward flow for the total transport and the layered transports. The total transport is positive (eastward) all year round with a maximum value of 45.7 Sv in January and a minimum value of 20.0 Sv in April with the annual mean transport of 34.4 Sv, which is consistent with Johnson and McPhaden's (1999) estimate (35 Sv) using the geostrophic calculations relative to a reference surface of 900 dbar.

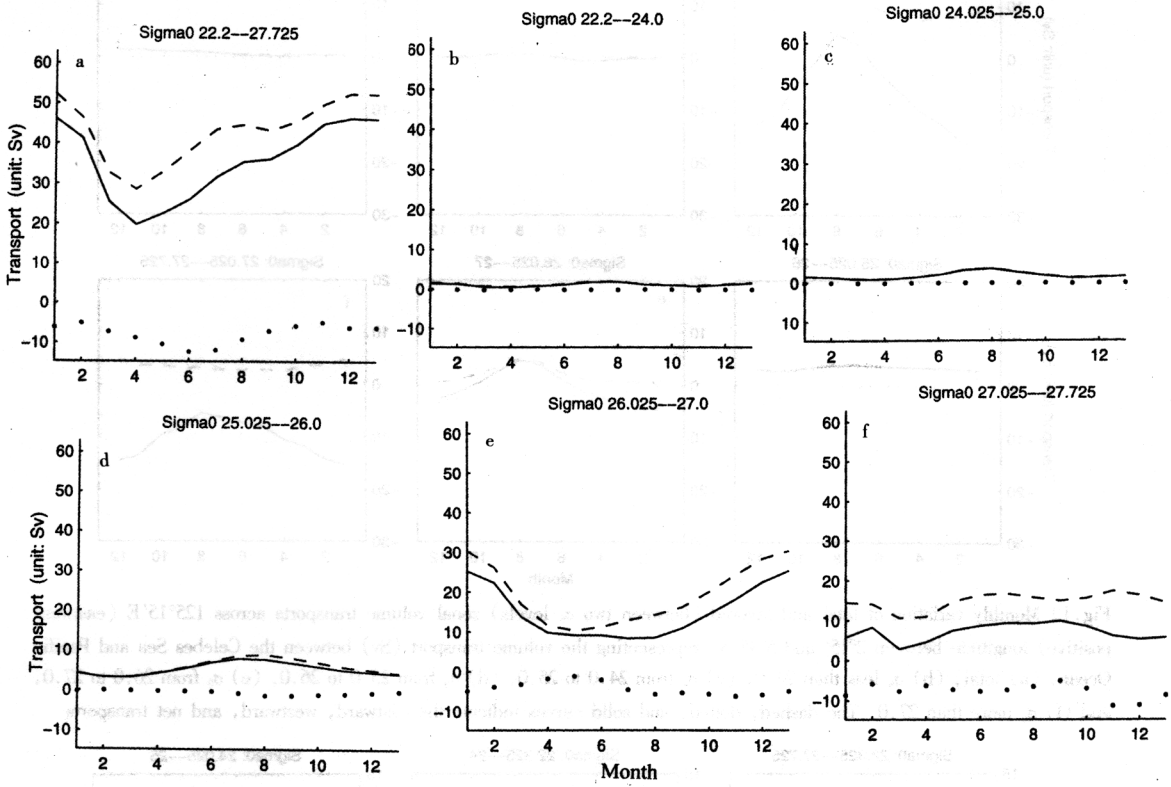

Fig. 12 Monthly variation of total and layered (between two σ_θ levels) zonal volume transports across 130°E longitude between 0°45′ and 6°15′N, representing the NECC transport (Sv). (a) total, (b) σ_θ less than 24.0, (c) σ_θ from 24.0 to 25.0, (d) σ_θ from 25.0 to 26.0, (e) σ_θ from 26.0 to 27.0, and (f) σ_θ more than 27.0. The dashed, dotted, and solid curves indicate the eastward, westward, and net transports

Volume transport to the Celebes Sea

We computed monthly total and layered (between two σ_θ levels) volume transports across 125° 15′E (eastward positive) between 2°15′ to 5°45′N latitude (Fig. 13) to represent the seasonal variability of volume transport to the Celebes Sea. The dashed, dotted, and solid curves indicate eastward, westward, and net transports. The eastward flow is much weaker than the westward flow for the total transport (denoting water entering the Celebes Sea) in January (− 16.7 Sv). The strength of the volume transport of MC into the Celebes Sea weakens from winter to spring, and in summer (August), the net transport (4.6 Sv) is eastward, indicating outflow from the Celebes Sea to the Pacific Ocean. The most layered transports are negative (westward) all year round except the mid-layer ($26.0 \leqslant \sigma_\theta \leqslant 25.025$), where the eastward flow is dominant.

Volume transport to the Molucca Sea

We computed monthly total and layered (between two σ_θ levels) volume transports across 1°45′N

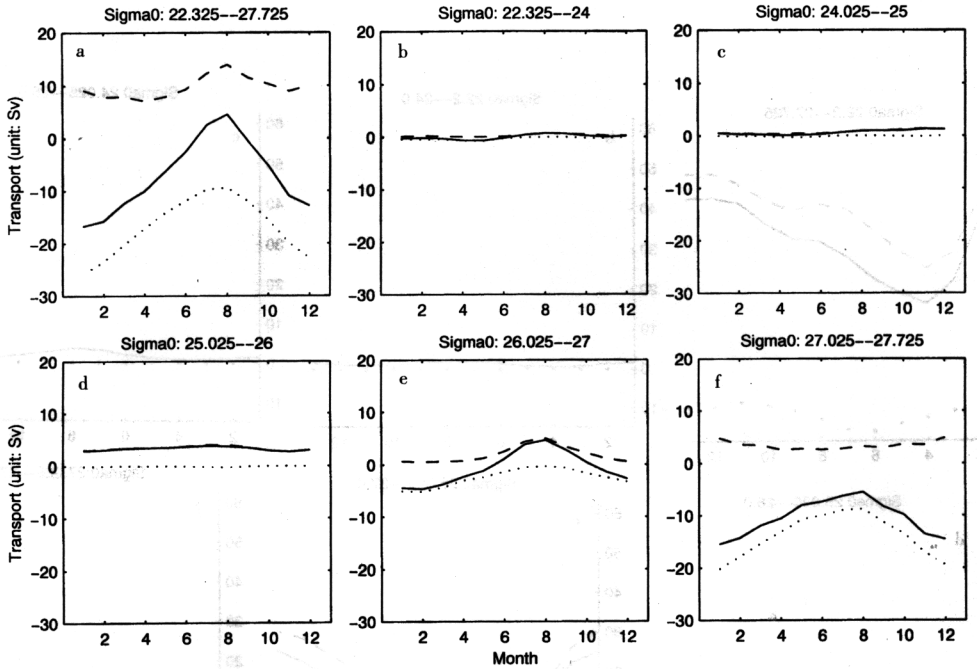

Fig.13 Monthly variation of total and layered (between two σ_θ levels) zonal volume transports across 125°15′E (eastward positive) longitude between 2°15′ and 5°45′N, representing the volume transport (Sv) between the Celebes Sea and Pacific Ocean. (a) total, (b) σ_θ less than 24.0, (c) σ_θ from 24.0 to 25.0, (d) σ_θ from 25.0 to 26.0, (e) σ_θ from 26.0 to 27.0, and (f) σ_θ more than 27.0. The dashed, dotted, and solid curves indicate the eastward, westward, and net transports

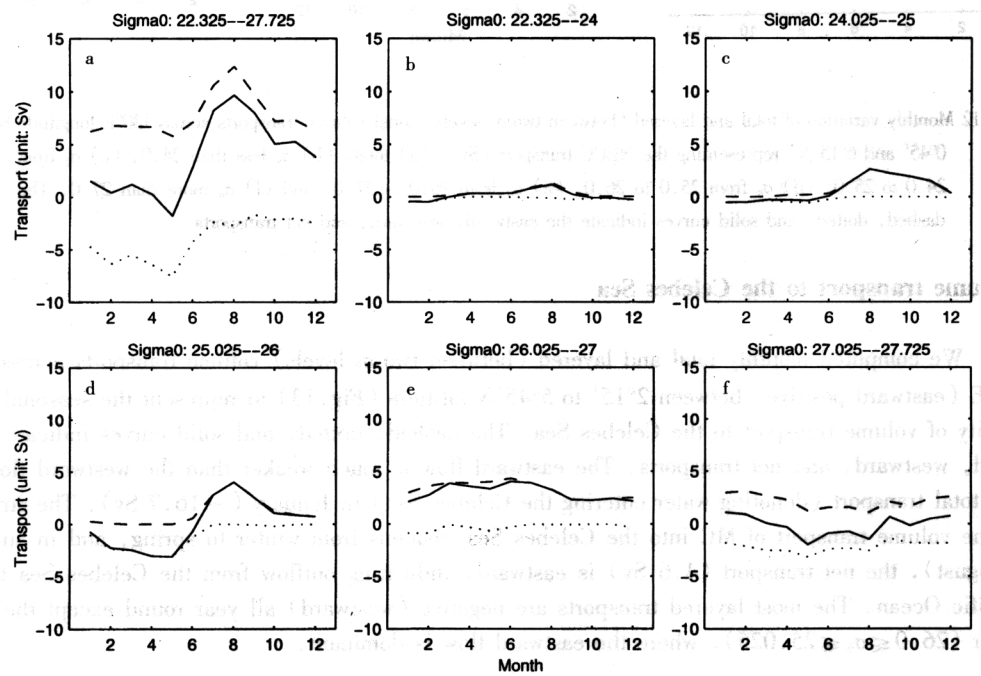

Fig.14 Monthly variation of total and layered (between two σ_θ levels) latitudinal volume transports (northward positive) across 1°45′N latitude between 125°45′ and 127°25′E, representing the seasonal varia bility of volume transport to the Molucca Sea. (a) total, (b) σ_θ less than 24.0, (c) σ_θ from 24.0 to 25.0, (d) σ_θ from 25.0 to 26.0, (e) σ_θ from 26.0 to 27.0, and (f) σ_θ more than 27.0. The dashed, dotted, and solid curves indicate the northward, southward, and net transports

(northward positive) between 125°45′ to 127°25′E longitude (Fig.14) to represent the seasonal variability of volume transport to the Molucca Sea. The dashed, dotted, and solid curves indicate northward, southward, and net transports. The southward flow (into the Molucca Sea) is a little weaker than the northward flow (out of the Molucca Sea) for the total transport in January (1.5 Sv). The net northward volume transport decreases with time. From February to May, the net volume transport is southward with the minimum value of −1.8 Sv in May. After May, the net volume transport becomes northward and enhances from 2.8 Sv in June to 7.9 Sv (maximum value) in August. The southward volume transport (into the Molluca Sea) is evident from January to June in the mid-layer ($26.0 \geqslant \sigma_\theta \geqslant 25.025$).

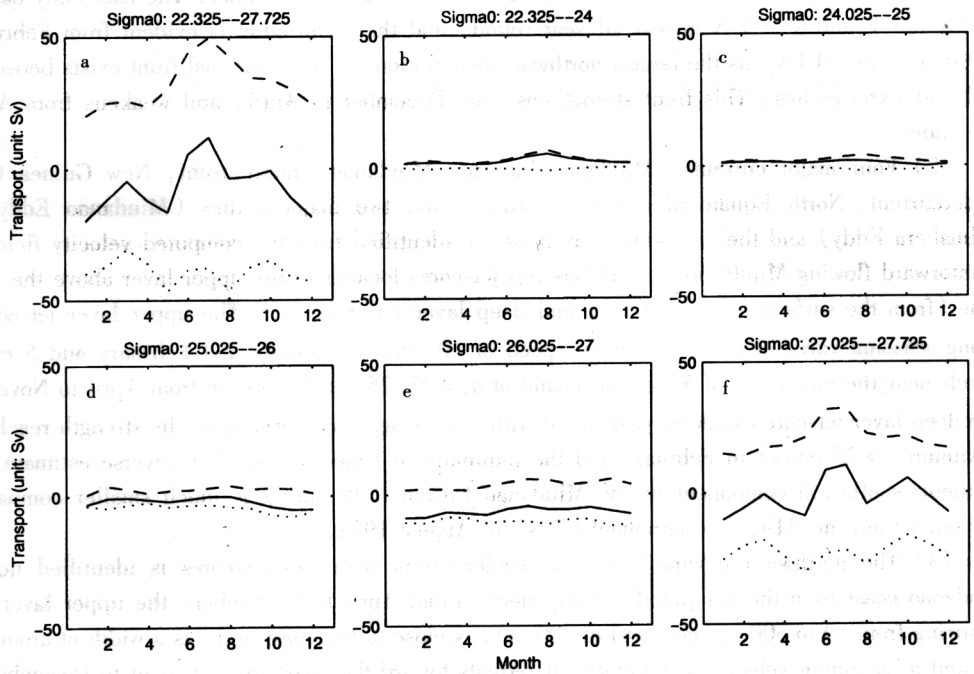

Fig.15 Monthly variation of total and layered (between two σ_θ levels) latitudinal volume transports (northward positive) across 1°45′N latitude between 129°30′ and 136°30′E, representing the seasonal variability of volume transport to the Halmahera Sea. (a) total, (b) σ_θ less than 24.0, (c) σ_θ from 24.0 to 25.0, (d) σ_θ from 25.0 to 26.0, (e) σ_θ from 26.0 to 27.0, and (f) σ_θ more than 27.0. The dashed, dotted, and solid curves indicate the northward, southward, and net transports

Volume transport to the Halmahera Sea

We computed monthly total and layered (between two σ_θ levels) volume transports across 1°45′N (northward positive) between 129°30′ to 136°30′E longitude (Fig.15) to represent the seasonal variability of volume transport to the Halmahera Sea. The dashed, dotted, and solid curves indicate northward, southward, and net transports. The southward flow (into the Halmahera Sea) is stronger than the northward flow (out of the Halmahera Sea) for the total transport in most of the year except in June and July. The net southward volume transport (into the Halmahera Sea) reaches the maximum strength (−19.6 Sv) in January. The net southward volume transport weakens from January to March (−4.5 Sv) and then strengthens from March to May (−16.4 Sv) with time. The net volume transport is positive (out of the Halmahera Sea) in June (5.6 Sv) and July (11.9 Sv). The net volume transport is southward from August (−3.5 Sv) to December (−18.2 Sv). The south-

ward volume transport (into the Halmahera Sea) is dominant in the deep layers ($27.0 \geqslant \sigma_\theta \geqslant 26.025$) and ($27.725 \geqslant \sigma_\theta \geqslant 27.025$).

5. CONCLUSIONS

(1) The GDEM data on the pycnocline layer ($\sigma_\theta = 25.0$) shows the cool (northern)-warm (southern) dipole eddy-like structure and the high-salinity SPTW ($\geqslant 35.0$ psu) co-located with the warm eddy. The SPTW expands toward the northwest in February – June with largest penetration in February – April, and retreats toward the southeast in August – December. The cool eddy occurs at 128° – 133°E and 6° – 9°N almost all year round, and the warm eddy is evident from February to April when the SPTW has the largest northward penetration. A weak thermal front exists between the cool and warm eddies. This front strengthens from December to April, and weakens from April to December.

(2) Four major currents (Mindanao Current, Mindanao Undercurrent, New Guinea Coastal Undercurrent, North Equatorial Counter Current) and two major eddies (Mindanao Eddy, and Halmahera Eddy) and their seasonal variations are identified from the computed velocity field. The equatorward flowing Mindanao Current has two jet-cores located in the upper layer above the pycnocline (from the surface to $\sigma_\theta = 25.0$), and deep layer ($\sigma_\theta > 26.5$). The upper layer jet-core has strong seasonal variability and maximum speed of 10 cm/s in January and February and 5 cm/s in March near the east coast of Mindanao Island at $\sigma_\theta = 23.25$. It disappears from April to November. The deep layer jet-core exists all year round with a weak seasonal variability. Its strength reaches the maximum (> 25 cm/s) in February and the minimum in June-August. The inverse estimate of the maximum southward component in the Mindanao Current (25 cm/s) is much smaller compared to 100 cm/s from the ADCP measurement (7°N) in August 1988.

(3) The northward flowing Mindanao Undercurrent with two jet-cores is identified near the Mindanao coast from the computed v-component. From April to September, the upper layer core, occurring from 50 to 300 m (centered at 200 m), is close to the coast and has a width of around 200 km and a maximum velocity of 10 cm/s. It retreats toward the coast from October to December with a width of less than 100 km, and expands toward the east to a longitude near 132°E from January to March with a maximum velocity (around 150 m depth). The lower layer core, occurring below 400 m, is around 100 km away from the coast and has weak seasonal variability in its location and strong seasonal variability in its strength. It reaches maximum strength (20 cm/s) in February and minimum strength (5 cm/s) from March to October.

(4) Both the Mindanao Eddy (cyclonic) and Halmahera Eddy (anticyclonic) are identified. In November, the Mindanao Eddy extends from 200 to 500 m with a jet core at 300 m depth. From November to March, its position keeps steady, but its strength varies drastically. The northward branch velocity increases to 20 cm/s in December and January, and the southward branch velocity increases to 25 cm/s in February. From April to October, the ME shifts southwestward to 128° – 133°E and south of 6°N. The Halmahera Eddy strengthens in Jun. – Aug. and weakens in December. The maximum westward speed in the southern flank of HE reaches 20 cm/s in June and July and 10 cm/s in February and March.

(5) The monthly total and layered (between two σ_θ evels) volume transport were computed along 7°15′N (northward positive) from the Mindanao coast to 130°45′E longitude to represent the seasonal transport variability of the Mindanao Current, and along 130°E (eastward positive) between 0°45′ and 8°15′N to represent the seasonal transport variability of the North Equatorial Counter Cur-

rent. The total transport of the Mindanao Current is equatorward all year round with a maximum value of 40.2 Sv in January and a minimum value of 5.3 Sv in June and July with the annual mean transport of 23.4 Sv, which agrees with many existing estimates. The total transport of the North Equatorial Countercurrent is eastward all year round with a maximum value of 45.7 Sv in January and a minimum value of 20.0 Sv in April with the annual mean transport of 34.4 Sv.

(6) The monthly total and layered volume transports were computed along 125°15′E (eastward positive) between 2°15′ to 5°45′N latitude to represent the seasonal variability of volume transport to the Celebes Sea. The net volume transport is into the Celebes Sea in most of the year, and has maximum strength in January (−16.7 Sv). It weakens from winter to spring, and in summer (August), the net transport (4.6 Sv) is out of the Celebes Sea into the Pacific Ocean. Most layered transports are negative (westward) all year round except the mid-layer ($26.0 \geqslant \sigma_\theta \geqslant 25.025$), where the eastward (out of the Celebes Sea) flow is dominant.

(7) The monthly total and layered volume transports were computed along 1°45′N (northward positive) between 125°45′ to 127°25′E longitude to represent the seasonal variability of volume transport to the Molucca Sea. The net volume transport is into the Molucca Sea from February to May with maximum strength in May (−1.8 Sv) and out of the Molucca Sea the rest of the year with maximum strength in August (7.9 Sv). The volume transport into the Molucca Sea is evident from January to June in the mid-layer ($26.0 \geqslant \sigma_\theta \geqslant 25.025$).

(8) The monthly total and layered volume transports were computed along 1°45′ (northward positive) between 129° to 13°30′E longitude to represent the seasonal variability of volume transport to the Halmahera Sea. The net volume transport is into the Halmahera Sea in most of the year except in June and July. The net volume transport into the Halmahera Sea reaches maximum strength (−19.6 Sv) in January. It weakens from January to March (−4.5 Sv) and then strengthens with time from March to May (−16.4 Sv). The net volume transport is out of the Halmahera Sea in June (5.6 Sv) and July (11.9 Sv). The net volume transport is into the Halmahera Sea again from August (−3.5 Sv) to December (−18.2 Sv). The volume transport into the Halmahera Sea is dominant in the deep layers ($27.0 \geqslant \sigma_\theta \geqslant 26.025$) and ($27.725 \geqslant \sigma_\theta \geqslant 27.025$).

ACKNOWLEDGEMENTS

Peter Chu and Chenwu Fan were supported by the Office of Naval Research and the Naval Oceanographic Office. Rongfeng Li was supported by the Natural Science Foundation of China (40076009), and Chinese Academy of Sciences (KZCX2-204, KZCX1-SW-01-16).

References

Bingham, F. M., Lukas, R., 1994. The Southward intrusion of North Pacific Intermediate Water along the Mindanao coast. *J. Phys. Oceanogr.* **24**: 141 – 154.

Bingham, F. M., Lukas, R., 1995. The distribution of intermediate water in the western equatorial Pacific during January – February 1986. *Deep – Sea Res.* **42**: 1545 – 1573.

Chu, P. C., 1995. P-vector method for determining absolute velocity from hydrographic data. *Mar. Tech. Soc. J.* **29**(3): 3 – 14.

Chu, P. C., 2000. P-vector spiral and determination of absolute velocities. *J. Oceanogr.* **56**: 591 – 599.

Chu, P. C., Fan, C. W., Cai, W. J., 1998a. Evaluation of P vector method using modular ocean model (MOM). *J. Oceanogr.* **54**: 185 – 198.

Chu, P. C., Fan, C. W., Lozano, C. J. et al., 1998b. An airborne expandable bathythermograph (AXBT) survey of the South China Sea, May 1995. *J. Geophys. Res.* **103**: 21637 – 21652.

Chu, P. C., Li, R. F., 2000. South China Sea isopycnal surface circulations. *J. Phys. Oceanogr.* **30**: 2419 – 2438.

Chu, P. C., Lan, J., Fan, C. W., 2001a. Japan Sea thermohaline structure and circulation, Part 1. Climatology. *J. Phys. Oceanogr.* **31**: 244 – 271.

Chu, P. C., Lan, J., Fan, C. W., 2001b. Japan/East Sea thermohaline structure and circulation, Part 2. A variational P-vector method. *J. Phys. Oceanogr.* **31**: 244 – 271.

Chu, P. C., Li, R. F., You, X. B., 2001c. Determination of Northern South China Sea isopycnal surface circulation using the P – vector method. *Adv. Natural Sci.* **11**: 499 – 506. (in Chinese)

Coatanoan, C., Metzl, N., Fieux, M. et al., 1999. Seasonal water mass distribution in the Indonesian throughflow entering the Indian Ocean. *J. Geophys. Res.* **104**: 20801 – 20826.

Ffield, A., Gordon, A. L., 1992. Vertical mixing in the Indonesian thermocline. *J. Phys. Oceanogr.* **22**: 184 – 195.

Fine, R. A., Lukas, R., Bingham, F. M. et al., 1994. The western equatorial Pacific – a water mass crossroads. *J. Geophys. Res.* **99**: 25063 – 25080.

Godfrey, J. S., 1996. The effect of the Indonesian throughflow on ocean circulation and heat exchange with the atmosphere. *A review. J. Geophys. Res.* **101**: 12217 – 12237.

Godfrey, J. S., Hirst, A. C., Wilkin, J., 1993. Why does the Indonesian throughflow appear to originate from the north Pacific? *J. Phys. Oceanogr.* **23**: 1087 – 1098.

Hu, D., Cui, M., 1989. The western boundary current in the far-western Pacific Ocean. *In*: Picaut, J., Lukas, R., Delcroix, T. (eds), Proceedings of the Western Pacific International Meeting and Workshop on TOGA COARE, ORSTOM, Noumea, New Caledonia, 24 – 30 May, p. 135 – 143.

Inoue, M., Walsh, S.E., 1993. Modeling seasonal variability in the wind-driven upper-layer circulation in the Indo-Pacific region. *J. Phys. Oceanogr.* **23**: 1411 – 1436.

Johnson, G. C., McPhaden, M. J., 1999. Interior pycnocline flow from the subtropical to the equatorial Pacific Ocean. *J. Phys. Oceanogr.* **29**: 3073 – 3089.

Kashino, Y., Aoyama M., Kawano, M. T. et al., 1996. The water masses between Mindanao and New Guinea. *J. Geophys. Res.* **101**: 12391 – 12400.

Kashino, Y., Watanabe, H., Herunadi, B. et al., 1999. Current variability at the Pacific entrance of the Indonesian Throughflow. *J. Geophys. Res.* **104**: 11021 – 11035.

Lukas, R., 1988. Interannual fluctuations of the Mindanao current inferred from sea-level. *J. Geophys. Res.* **93**: 6744 – 6748.

Lukas, R., Firing, E., Hacker, P. et al., 1991. Observations of the Mindanao current during the western equatorial Pacific-Ocean circulation study. *J. Geophys. Res.* **96**: 7089 – 7104.

Lukas, R., Yamagata, T., McCreary, J. P., 1996. Pacific low-latitude western boundary currents and the Indonesian throughflow. *J. Geophys. Res.* **101**: 12209 – 12216.

Masumoto, Y., Yamagata, T., 1991. Response of the western tropical Pacific to the Asian winter monsoon – The generation of the Mindanao dome. *J. Phys. Oceanogr.* **21**: 1386 – 1398.

Masuzawa, J., 1969. The Mindanao Current. *Bull. Jpn. Soc. Fish. Oceanogr. Spec. No. Prof. Uda's Comm. Pap.* p. 99 – 104.

McDougall, T. J., 1988. Neutral-surface potential vorticity. *Prog. Oceanogr.* **20**: 185 – 221.

McDougall, T. J., 1995. The influence of ocean mixing on the absolute velocity vector. *J. Phys. Oceanogr.* **25**: 705 – 725.

Metzger, E. J., Hurlburt, H. E., 1996. Coupled dynamics of the South China Sea, the Sulu Sea, and the Pacific Ocean. *J. Geophys. Res.* **101**: 12331 – 12352.

Miyama, T., Awaji, T., Akitomo, K. et al., 1995. Study of seasonal transport variations in the Indonesian seas. *J. Geophys. Res.* **100**: 20517 – 20541.

Qiu, B., Lukas, R., 1996. Seasonal and interannual variability of the North Equatorial Current, the Mindanao Current, and the Kuroshio along the Pacific western boundary. *J. Geophys. Res.* **101**: 12315 – 12330.

Qiu, B., Mao, M., Kashino, Y., 1999. Intraseasonal variability in the indo-pacific throughflow and the regions surrounding the Indonesian seas. *J. Phys. Oceanogr.* **29**: 1599 – 1618.

Qu, T. D., Mitsudera, H., Yamagata, T., 1998. On the western boundary currents in the Philippine Sea. *J. Geophys. Res.* **103**: 7537 – 7548.

Qu, T. D., Mitsudera, H., Yamagata, T., 1999. A climatology of the circulation and water mass distribution near the Philippine coast. *J. Phys. Oceanogr.* **29**: 1488 – 1505.

Shriver, J. F., Hurlburt, H. E., 1997. The contribution of the global thermohaline circulation to the Pacific to Indian Ocean throughflow via Indonesia. *J. Geophys. Res.* **102**: 5491 – 5511.

Teague, W. J., Carron, M. J., Hogan, P. J., 1990. A comparison between the Generalized Digital Environmental Model and Levitus climatology, *J. Geophys. Res.* **95**: 7167 – 7183.

Wajsowicz, R. C., 1993. A simple-model of the Indonesian throughflow and its composition. *J. Phys. Oceanogr.* **23**: 2683 – 2703.

Wajsowicz, R. C., 1999a. Models of the Southeast Asian seas. *J. Phys. Oceanogr.* **29**: 986 – 1018.

Wajsowicz, R.C., 1999b. Variations in gyre closure at the water mass crossroads of the western equatorial Pacific Ocean. *J. Phys. Oceanogr.* **29**: 3002 – 3024.

Wijffels, S. E., Firing, E., Toole, J., 1995. The mean structure and variability of the Mindanao current at 8°N. *J. Geophys. Res.* **100**: 18421 – 18435.

Wyrtki, K., 1961. Physical oceanography of the Southeast Asian Waters, Naga Rep. Scripps Institution of Oceanography, University of California, San Diego, **2**: 195 pp.